JGR Space Physics

Key Points:
- Santa Maria Digisonde data acquired in the SAMA center are used for the first time to study a geomagnetic storm (August 25, 2018)
- Positive and negative ionospheric storm effects are detected at different latitudes along the American sector during the early recovery phase on August 26
- Large enhancement of plasma density is observed in the southern crest of the Equatorial Ionization Anomaly during the recovery phase

Correspondence to:
J. Moro,
juliano.moro@inpe.br;
julianopmoro@gmail.com

First Look at a Geomagnetic Storm With Santa Maria Digisonde Data: *F* Region Responses and Comparisons Over the American Sector

J. Moro[1,2] , J. Xu[1] , C. M. Denardini[3] , L. C. A. Resende[1,3] , P. F. Barbosa Neto[3,4] , L. A. Da Silva[1,3] , R. P. Silva[3] , S. S. Chen[3] , G. A. S. Picanço[3] , C. S. Carmo[3] , Z. Liu[1] , C. Yan[1] , C. Wang[1] , and N. J. Schuch[2]

[1]State Key Laboratory of Space Weather, Beijing, China, [2]Southern Space Coordination-COESU/INPE/MCTI, Santa Maria, Brazil, [3]Space Weather Division, National Institute for Space Research-INPE/MCTI, São José dos Campos, Brazil, [4]Faculty of Production Engineering, Salesian University Center of São Paulo, Lorena, Brazil

Abstract Santa Maria Digisonde data are used for the first time to investigate the *F* region behavior during a geomagnetic storm. The August 25, 2018 storm is considered complex due to the incidence of two Interplanetary Coronal Mass Ejections and a High-Speed Solar Wind Stream (HSS). The F_2 layer critical frequency (f_oF_2) and its peak height (h_mF_2) collected over Santa Maria, near the center of the South American Magnetic Anomaly (SAMA), are compared with data collected from Digisondes installed in the Northern (NH) and Southern (SH) Hemispheres in the American sector. The deviation of f_oF_2 (Df_oF_2) and h_mF_2 (Dh_mF_2) are used to quantify the ionospheric storm effects. Different *F* region responses were observed during the main phase (August 25–26), which is attributed to the traveling ionospheric disturbances and disturbed eastward electric field during nighttime. The *F* region responses became highly asymmetric between the NH and SH at the early recovery phase (RP, August 26) due to a combination of physical mechanisms. The observed asymmetries are interpreted as caused by modifications in the thermospheric composition and a rapid electrodynamic mechanism. The persistent enhanced thermospheric [O]/[N_2] ratio observed from August 27 to 29 combined with the increased solar wind speed induced by the HSS and IMF B_z fluctuations seem to be effective in causing the positive ionospheric storm effects and the shift of the Equatorial Ionization Anomaly crest to higher than typical latitudes. Consequently, the most dramatic positive ionospheric storm during the RP occurred over Santa Maria (~120%).

Plain Language Summary The SAMA is a sector of a global minimum in the geomagnetic field total intensity. Currently, it covers a big portion of Brazil. Ground-based and satellite measurements have detected elevated levels of highly energetic particles in the SAMA, which has practical consequences for satellite design and operation as well as it is of great concern to astronauts crossing the geomagnetic anomaly. Moreover, the plasma density may be intensified or decreased in low and middle latitude regions during geomagnetic storms which, in turn, impose additional problems in satellite communication, navigation, and serious radio block out in ground-based high-frequency communication. Therefore, the ionosphere behavior over the SAMA in Brazil presents some unique geophysical characteristics. In this work, analysis of the recent Digisonde data collected in Santa Maria, in SAMA center, will permit the study of the drivers acting in changing the electron density during the August 25, 2018 geomagnetic storm. The results are compared with data from Digisondes installed in the NH and SH in the American sector, inside and outside the influence of the SAMA. Among the stations, Santa Maria presented the highest deviations.

1. Introduction

The ionosphere-thermosphere (I-T) responses are an important research topic in space weather during storm-time when two basic types of disturbed ionospheric electric fields are known to occur. The first one is popularly referred as "prompt penetration electric field" (PPEF; Kikuchi et al., 2000). It is transmitted almost instantaneously to the equatorial latitudes as an "undershielding" process having eastward (westward) direction on the dayside (nightside) of the Earth (Wolf et al., 2007). During daytime hours, the PPEF

of eastward polarity can uplift the equatorial ionosphere, and consequently, there are intensifications of the Equatorial Plasma Fountain (EPF) and the poleward expansion of the Equatorial Ionization Anomaly (EIA) crests (Balan et al., 2017; Balan & Bailey, 1995; Fagundes et al., 2016; Sobral et al., 2001; Tsurutani et al., 2004). The PPEF also causes the intensification in the Pre-Reversal Enhancement (PRE) vertical drift. The sudden increment in the layer height may give rise to the Rayleigh-Taylor instability and the development of spread-F irregularities (Abdu et al., 2008; Li et al., 2010). If the IMF B_z component suddenly changes direction and turns northward, the "overshielding" condition takes place, and the region-2 field-aligned current over shields the region-1 current from now-weakened convection. As a result, the dawn-to-dusk electric field is oriented in dusk-to-dawn direction in the inner magnetosphere (Kelley et al., 1979). The overshielding westward electric field at nighttime can also be intense to cause a suppression of the PRE and spread-F irregularities (Abdu et al., 2009). The second type of disturbing electric field is called "disturbance wind dynamo electric field" (DDEF; Blanc & Richmond, 1980). During the dayside (nightside) of the Earth, the DDEF is westward (eastward), i.e., contrary to the ordinary ionospheric dynamo. The study of DDEF is also important because it may cause the (total or partial) suppression of the EIA in the daytime hours during the recovery phase (RP) of geomagnetic storms (Balan et al., 2013). On the other hand, the eastward polarity of DDEF during nighttime hours can uplift the F layer in the equatorial region and enhance the electron density in the EIA crests region (15º–20º in the north and the south geomagnetic latitude). Joule dissipation at high latitudes also modifies the thermospheric concentration. The electron density is governed by the photoionization of atomic oxygen density [O] and loss with molecular nitrogen [N_2] and oxygen [O_2]. Thus, the F region electron density is directly proportional to the thermospheric [O]/[N_2] ratio when the transport is not important (Danilov, 2013; Yu et al., 2020).

The previous competing drivers (ionospheric disturbed electric fields and the thermospheric composition) usually cause global modifications in the F_2 layer critical frequency (f_oF_2, representing the peak electron density N_mF_2) and its peak height (h_mF_2) relative to some quiet-time background level. The increase of the f_oF_2 concerning the quiet days is widely known as positive ionospheric storm. It is explained in terms of several physical mechanisms, among others, the increase in the atomic oxygen, disturbed electric fields, and Traveling Atmospheric/Ionospheric Disturbances (TAD/TID) (Fuller-Rowell et al., 1996; Huang et al., 2005). Contrarily, a decrease of f_oF_2 during storm-time is known as negative ionospheric storm and it may be caused by a decrease in the thermospheric [O]/[N_2] ratio (Danilov, 2013; Prölss, 1995; Zhang et al., 2003).

Some review articles on ionospheric storms (i.e., Prölss, 1995; Danilov, 2013, and reference therein) have reported examples of serious problems in satellite communication and navigation during severe positive storms effects. On the other hand, severe negative storms can cause serious radio block out in ground-based high-frequency communication. Therefore, more than ever, a robust understanding of the positive and negative ionospheric storms is important in the anomalously low geomagnetic field intensity region currently located in South America known as South American Magnetic Anomaly (SAMA; Abdu et al., 2005; Kurnosova et al., 1962). In addition to positive/negative phases observed in the electron density that may cause problems in satellites, the large high-energy particles that penetrate in the ionosphere may cause problems in satellite sensors (Schuch et al., 2019). It was also reported that the operator who controls satellites in low-Earth orbit may need to turn sensors off to reduce the detector saturation when passing through the SAMA (Jones et al., 2017). The energetic particles also enhance the ionization distribution and conductivities in the SAMA during geomagnetic storms (Moro et al., 2012; 2013).

As can be noted, the ionosphere-thermosphere (I-T) response in the SAMA region is an important research topic in space weather, especially during storm-time. It can be understood better by studying individual cases since any geomagnetic storm has its specific characteristics and, therefore, each case needs an individual approach (Astafyeva et al., 2020; Blagoveshchensky & Sergeeva, 2020). Although many case studies, statistics, and model simulations have reported the effects of geomagnetic storms in the I-T system everywhere in the globe, the drivers acting in changing the electron density in the SAMA are a poorly explored research topic. The data collected from a Digisonde installed in Santa Maria, near the SAMA center, permit now these studies that are otherwise unachieved. The selected disturbed period is the first one in which Santa Maria Digisonde data are available in all phases of the storm. The August 25, 2018 geomagnetic storm is considered very complex by several authors (Abunin et al., 2020; Astafyeva et al., 2020) since it was caused
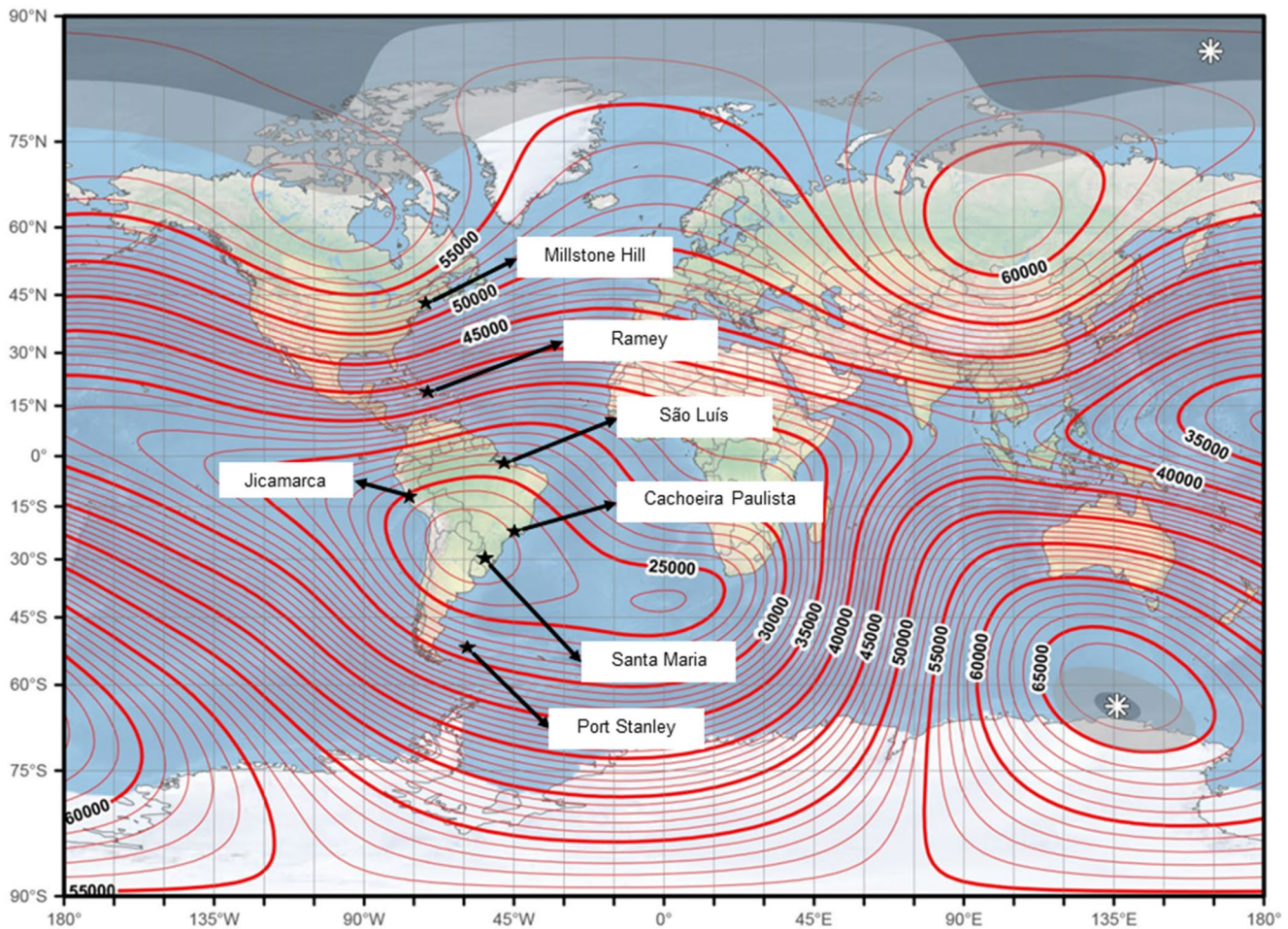
Figure 1. Global map with the geomagnetic field total intensity. The South American Magnetic Anomaly (SAMA) position is defined by the lowest iso-intensity line (23,000 nT) currently located in South America. The contour interval is 1,000 nT. The map also shows the different ionosonde stations used in this work. Source: Modified from Chulliat et al. (2020).

by two consecutive Interplanetary Earth-directed Coronal Mass Ejections (ICMEs) and a followed High-Speed Solar Wind Stream (HSS).

Thus, this work aims to study the *F* region responses over Santa Maria during the August 25, 2018 geomagnetic storm, the third most intense of the Solar Cycle 24. The geographical and geomagnetical extension of the drivers responsible for the storm-time *F* region behavior is analyzed by comparing ionospheric data acquired from digital ionosondes installed outside the influence of SAMA in the Northern (NH) and Southern (SH) Hemispheres within the American sector.

2. Data Presentation and Method of Analysis

Figure 1 shows the Digisonde (DPS-4D) map with the stations used in this work with respect to their position to the SAMA. The red lines in the map are the iso-intensity lines of the total geomagnetic field provided by the World Magnetic Model (WMM; Chulliat et al., 2020). The line with 23,000 nT defines the position of the anomaly center. It should be noted that out of seven stations shown on the map, Santa Maria and Cachoeira Paulista are located inside the iso-line of 23,000 nT and very close to it, respectively. The shape of the SAMA is asymmetric (Zou et al., 2015) and covers most of South America, from West Africa to the Pacific Ocean, and from the equator to Antarctica. Its center is located nowadays in Paraguay.

In Santa Maria, ionospheric sounding using Digisonde began in April 2017. The variability of f_oF_2, h_mF_2, E region critical frequency (f_oE), and the thickness parameter $B0$ was reported by Moro et al. (2019). In a recent work, Moro et al. (2020) compared the observed f_oF_2, h_mF_2, and f_oE collected during geomagnetically quiet days with the International Reference Ionosphere (IRI) outputs. The Digisondes installed at São Luís and Cachoeira Paulista belong to the Embrace Digisonde Network (DigiNet; Denardini et al., 2016). All necessary information about the Digisondes relevant to this work is shown in Table 1.

The Digisonde stations are distributed from middle, low, and equatorial latitude regions in the NH (Millstone Hill and Ramey) and the SH (São Luís, Jicamarca, Cachoeira Paulista, Santa Maria, and Port Stanley). As mentioned by Denardini et al. (2016), there is no exact definition where the boundaries of these regions are located. Therefore, in this work, it means that 5°N ≤ geomagnetic latitude ≤ 5°S is an equatorial region (Jicamarca), 5° < geomagnetic latitude < 20° is low latitude (São Luís and Cachoeira Paulita), and 20° < geomagnetic latitude < 50º is middle latitude (Santa Maria, Port Stanley, Millstone Hill, and Ramey). It is seen that São Luís and Santa Maria stations are currently located in a transition region from equatorial to low, and low to middle latitude region, respectively, due to the northwestward movement of the geomagnetic equator (Moro et al., 2017; Resende et al., 2016).

The Digisonde data came from the GIRO Digital Ionogram DataBase (DIDBase; http://umlcar.uml.edu/, Reinisch & Galkin, 2011). The ionospheric effects in the F region are investigated using the f_oF_2 and h_mF_2 parameters. The relative deviations of these ionospheric parameters are used to quantify the electronic density and height variations over each station. The relative deviation of the parameter f_oF_2, Df_oF_2, is defined in percent by $Df_oF_2 = 100 \, (f_oF_2 - f_oF_2(q))/f_oF_2(q)$, where f_oF_2 is the parameter measured during the storm-time. The day-to-day variability is removed with the mean quiet level ($f_oF_2(q)$) obtained using the data acquired during the five International Quiet Days (IQDs) of the month. The range of ±20% in Df_oF_2 is used by several authors (Habarulema et al., 2020; Matamba et al., 2015, and reference therein) to represent the day-to-day variability, and the deviations outside this range are attributed to the ionospheric disturbances during the geomagnetic storms. The five IQDs used in this work are August 6, 10, 13, 14, and 23, 2018, except for Port Stanley which used September 1, 3, 8, 19, and 20, 2018 due to the lack of measurements. Positive Df_oF_2 values correspond to the existence of positive ionospheric storms. A similar relation was considered for the relative deviation of the peak height h_mF_2, Dh_mF_2.

It is also used in this work the thermospheric column-integrated $[O]/[N_2]$ from the Global Ultraviolet Imager (GUVI) spectrograph of the TIMED satellite (http://guvitimed.jhuapl.edu/; Christensen et al., 2003; Paxton et al., 2005). The effects of the solar wind plasma and the IMF in the Earth space environment from August 25 to 29, 2018 are analyzed with observations of the Advanced Composition Explorer (ACE) satellite in the Lagrange point L1. The data are downloaded from the OMNI Website all at a 1-minute resolution (http://omniweb.gsfc.nasa.gov/). The convective IEF east-west E_y component (i.e., the dawn-to-dusk component) is derived using the following expression (in geocentric solar magnetospheric coordinates): $IEF \, E_y = (V_x)(IMF \, B_z)$, given in mV/m. The symmetric and asymmetric component of ring current (*SYM-H*, *ASY-H*, both in nT) indexes come from the World Data Center from Geomagnetism, Kyoto. Regarding the start times of the disturbances, they are taken from the ICMEs catalog maintained by Richardson and Cane (R&C; Richardson & Cane, 2010, http://www.srl.caltech.edu/ACE/ASC/DATA/level3/icmetable2.htm).

3. Description of the Complex Interplanetary and Geomagnetic Conditions from August 25 to 29, 2018

An unexpected and unusual strong geomagnetic storm (G3 class storm accordingly to the NOAA Space Weather Prediction Center) occurred on August 25, 2018. The analysis performed by Abunin et al. (2020) revealed that the storm was initiated by a two-step long filament eruption in the central sector of the solar disk on August 20. It was accompanied by two consecutive ICMEs of a rather small size and low speed and followed by the HSS. The interaction of this first solar wind structure created a strong compression of the Earth's magnetosphere, in which the magnetopause standoff distance (R_{mp}) calculated by an empirical model (Shue et al., 1998) reached ~7 Earth radius (R_E = 6,371 km). It means that the outer and inner magnetosphere was considerably perturbed during the influences of these ICMEs (Alves et al., 2016), and, consequently, the ionosphere may have been suffered influences of this magnetopause compression.

Table 1
Characteristics of Ionosondes Stations Used in This Work

|	Station						
	Millstone Hill	Ramey	São Luis	Jicamarca	Cachoeira Paulista	Santa Maria	Port Stanley
URSI code	MHJ45	PRJ18	SAA0K	JI91J	CAJ2M	SMK29	PSJ5J
GLAT (+N)	42.6°	18.5°	−2.6°	−12.0°	−22.7°	−29.7°	−51.6°
GLON (W)	71.5°	67.1°	44.2°	76.8°	45.0°	53.8°	57.9°
Geomagnetic latitude (+N)	51.9°	27.9°	5.8°	−2.4	−14.0°	−20.5°	−42.2°
Geomagnetic longitude (W)	1.4°	5.9°	28.6°	4.1°E	26.3°	17.5°	12.4°
Dip angle	67°	43°	−11°	−0.8	−39°	−37°	−50°
Total magnetic field (nT)	51,925	37,028	26,177	24,800	23,064	22,374	28,051
Time resolution (minutes)	15	5	10	15	10	5	30
UTC offset	−4 h	−3 h	−3 h	−5 h	−3 h	−3 h	−3 h
Sunrise* (UT)	10:00	9:08	8:57	11:14	9:16	9:58	10:43
Sunset* (UT)	23:28	21:44	21:00	23:03	20:47	21:16	21:04

*On 25 August 2018.

The solar wind parameters measured by the instruments onboard the ACE satellite are shown from top to bottom in Figures 2a–2d. The R_{mp} obtained with the model developed by Shue et al. (1998) is shown in Figure 2a (olive line). The estimated dawn to dusk IEF E_y component is shown in Figure 2e. The *SYM-H* and *ASY-H* (blue line) indexes are shown in Figure 2f. The vertical dotted lines identified as IP, MP, and RP mark the initial phase, the main phase, and the recovery phase, respectively.

The R&C catalog reports that the ICME shock arrived at Earth at 2:00 UT on August 20, 2018, when the solar wind pressure P_{SW} (Figure 2a), proton density N_p (Figure 2b), solar wind speed V_{SW} (Figure 2c), and the IMF B (Figure 2d) increased. The shock did not cause a sudden geomagnetic impulse in the *SYM-H* index (Figure 2f). The positive IMF B_z component (Figure 2d) started to decrease and changed to negative values at ∼16:00 UT and continued for a long duration (∼18 h) in the southward direction before recovering. At the same time, the R_{mp} started to decrease (Figure 2a, olive line) and achieved ∼7 R_E at around 4 UT. The IEF E_y component (Figure 2e) changed from negative (westward) to positive (eastward) values at 16:00 UT, while V_{SW} (Figure 2c) was stable around 430 km/s. The ring current became energized causing a drop of the *SYM-H* index (Figure 2f). Simultaneously, the enhancement of the auroral electrojet caused an increase in the *ASY-H* index. The IEF E_y remained positive (eastward) and rose to the maximum values of 7.5 mV/m at 5:00 UT on August 26. At the same time, the IMF B_z achieved its lowest value of −18 nT, and *ASY-H* rose to its maximum value of 198 nT. The *SYM-H* index reached its minimum value of −206 nT two hours later, at ∼7:00 UT. After that, the geomagnetic storm goes into the RP.

The increase in P_{SW} (Figure 2a), N_p (Figure 2b), and V_{SW} (Figure 2c) at around 8:00 UT on August 26 signals the HSS. A fairly strong IMF B (Figure 2d) equal to 19 nT was detected at 9:20 UT on August 26. The presence of two enhancements of pressure (Figure 2a) and density (Figure 2b) at 04:00–06:00 UT and 13:00 UT on 26 August reflects the complex structure. New and strong intensifications were observed in the IMF B_z at 9:57 UT (3.18 nT), 13:09 UT (16.07 nT), 18:12 UT (10.33 nT), and 20:28 UT (4.32 nT) identified as 1, 2, 3, and 4, respectively. Similar to the IMF B_z, the peaks also appeared in IEF E_y. The auroral electrojet became more intense as represented by several peaks in the *ASY-H* index. The *SYM-H* also exhibited two peaks (2, 3 in Figure 2f) marking the first changes in the recovery slope. These peaks coincide with the Peaks 2 and 3 of the IMF B_z.

During the influences of the HSS, the V_{SW} increased (from ∼380 km/s to ∼580 km/s) between 7:00 UT on August 26 and 6:00 UT on August 27, followed by a second enhancement in which V_{SW} plateaued around 630 km/s at 17:00 UT on August 27. After that, V_{SW} started to decrease until it achieved ∼450 km/s on August 29. IMF features observed from August 27 suggest the presence of the Alfvénic fluctuations, as B_x, B_y
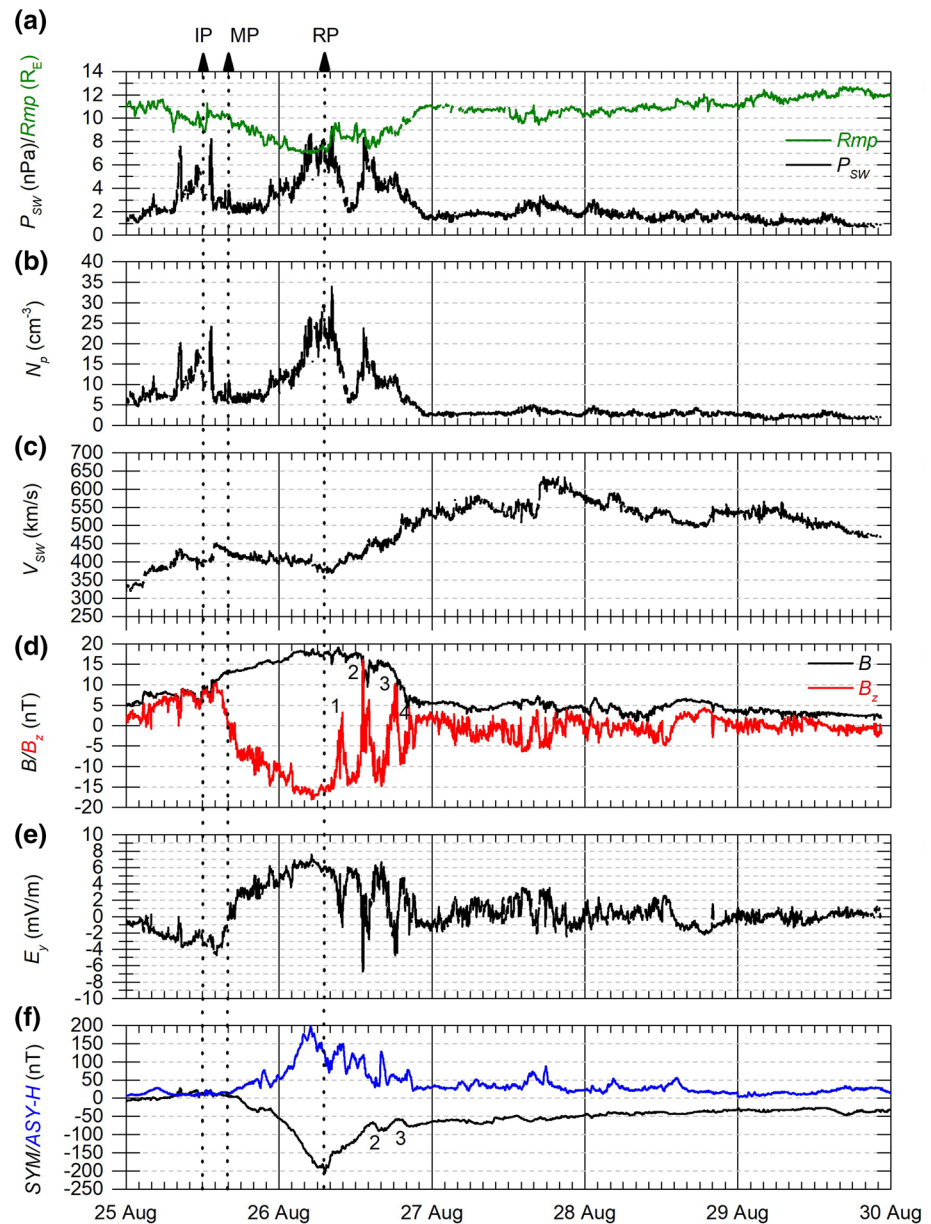
Figure 2. Interplanetary and geophysical parameters from August 25 to 29, 2018 geomagnetic storm: (a) solar wind pressure P_{SW} (black line) and magnetopause standoff distance R_{mp} (olive line), (b) solar wind proton density N_p, (c) solar wind speed V_{SW}, (d) IMF B (black line) and north-south IMF B_z component (red line) in GSM coordinate, (e) estimated dawn to dusk IEF E_y component, and (f) asymmetric ring current ASY-H (blue line) and symmetric ring current SYM-H (black line) indexes. The vertical dotted lines and labels indicate the initial (IP; 12:00 UT), main (MP; 16:00 UT), and recovery (RP; 7:00 UT) phases of the geomagnetic storm, respectively.

(figure not shown), and B_z fluctuated greatly, and also because the IMF B_z component presented orientation on average southward. These features in IMF components occurred concomitantly with low density (Figure 2b) in the interplanetary medium, and with the R_{mp} relaxed (~10 R_E). The SYM-H continued to grow slowly and recovered to 10% of its lowest value at around 23:00 UT on August 29. The total recovery of the SYM-H index to the prestorm level occurred on September 1. The maximum solar extreme ultraviolet flux proxy F10.7 (measured in sfu = 10^{-22} Wm^{-2}Hz^{-1}) during this geomagnetic storm was 74.
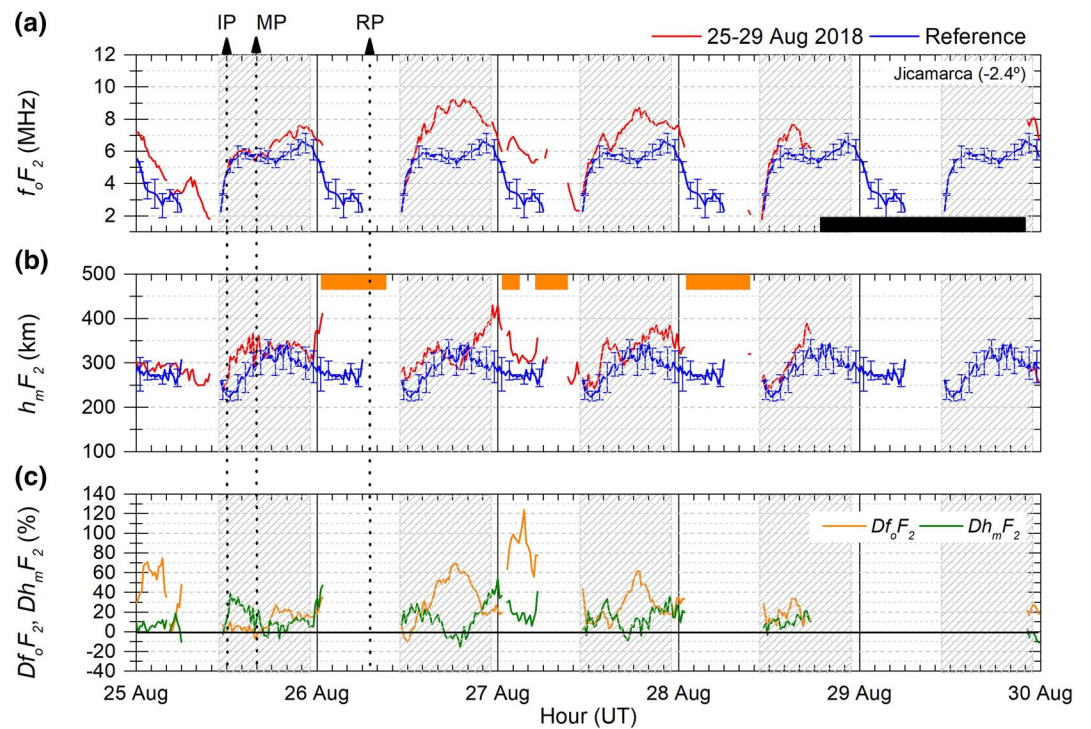
Figure 3. Observed (a) f_oF_2 and (b) h_mF_2 (blue lines) and the respective averaged quiet days (blue curves) and (c) Df_oF_2 (orange line) and Dh_mF_2 (green line) at Jicamarca. The vertical dotted lines and labels indicate the initial (IP; 12:00 UT), main (MP; 16:00 UT), and recovery (RP; 7:00 UT) phases of the geomagnetic storm, respectively. The gray areas correspond to the local daytime hours. The Jicamarca Digisonde did not operate during some hours between August 28 and 29, as shown by the black rectangle in panel (a). The presence of spread-F in the ionograms are represented by the orange rectangles in panel (b).

4. Results and Discussions

Figure 3 shows from the top panel to bottom the observed f_oF_2 and h_mF_2 parameters and their respective deviations from August 25 to 29, 2018 over Jicamarca. The vertical dotted lines marked as IP, MP, and RP mark the phases of the geomagnetic storm. The gray hatched areas show the local day hours (see Table 1 for specific sunrise and sunset hours on August 25, 2018). The red line represents the parameter during storm-time. The blue line is the averaged quiet days, in which error bars are plotted only hourly to avoid overcrowding. The comparison between the storm-time f_oF_2 and the averaged quiet days (Figure 3a) is particularly useful to show the manifestation of positive/negative storms. On the other hand, the variation of h_mF_2 with respect to the reference level (Figure 3b) is used to identify the possible action of an electrodynamic source (disturbed electric fields) acting in uplift or decrease the F layer in relation to the ground. It is also noticeable that there is no evening peak in the reference h_mF_2 over Jicamarca. This behavior was reported before by Lee et al. (2008). The presence of spread-F in the ionograms are marked by horizontal orange bars, whereas the black ones show no data collected by the Digisonde.

The f_oF_2 and h_mF_2 for the remaining stations are presented in Figures 4 and 5, respectively. These figures follow the same pattern described in Figure 3 and are arranged from top to bottom in decreasing order of geomagnetic latitude. A first look at these results reveals similarities and differences in the American sector. Their quantitative descriptions are presented in terms of the relative deviations Df_oF_2 (orange line) and Dh_mF_2 (green line) for Jicamarca in Figure 3c, and in remaining stations in Figure 6.

Regarding the experimental data (red lines), one can notice gaps in the curves. They occurred due to several reasons: over Millstone Hill (51.9º) and Ramey (27.9º) they are mainly caused by the total or partial absence of the reflecting echoes in ionogram which, in turn, is associated to a decrease of f_oF_2 observed during the negative ionospheric storm; over Port Stanley (−42.2º), the gaps are caused by the lack of measurements
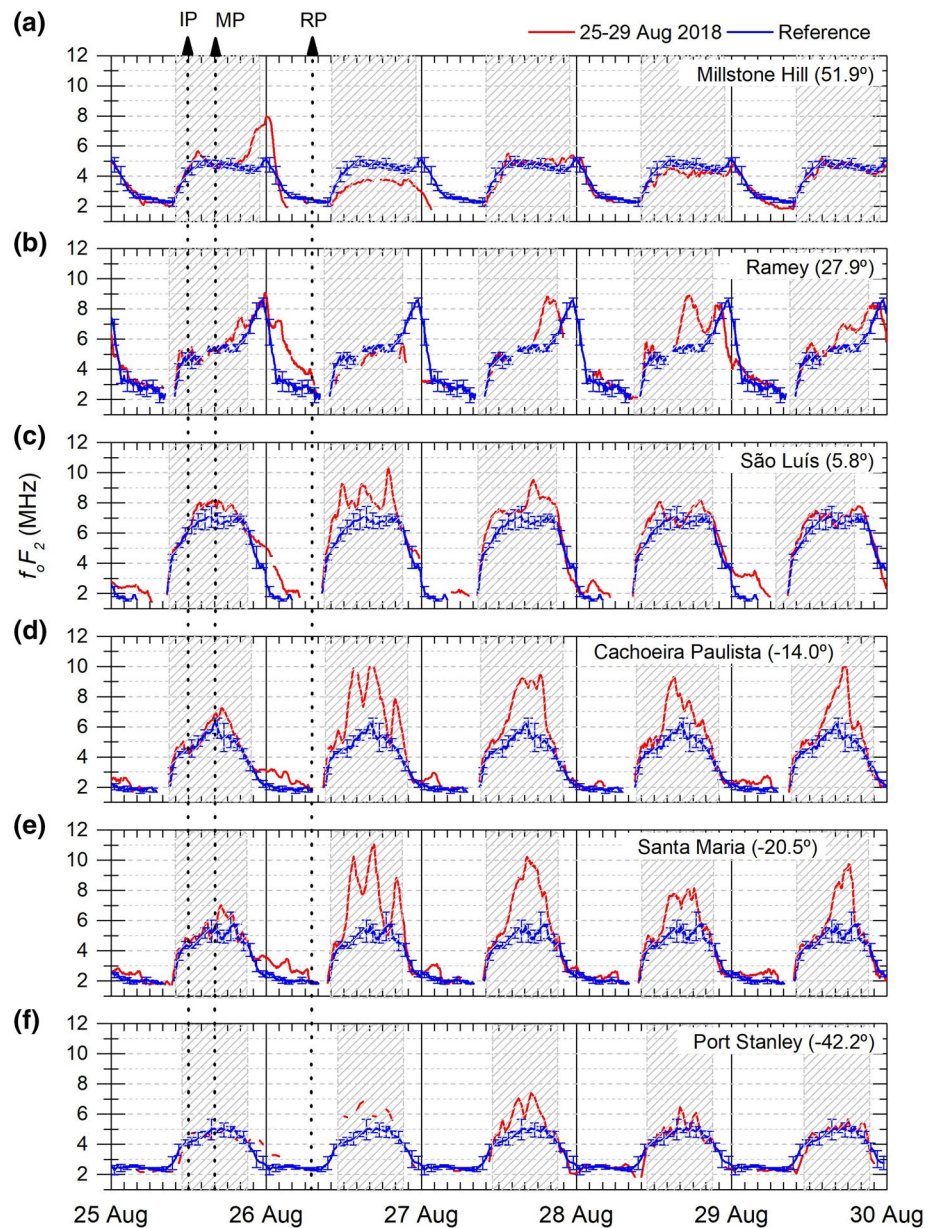
Figure 4. f_oF_2 from August 25 to 29, 2018 (red curves) with respect to the averaged quiet days (blue curves) at (a) Millstone Hill (b) Ramey (c) São Luís (d) Cachoeira Paulista (e) Santa Maria, and (f) Port Stanley.

(associated with the relatively low resolution—30 min—set in the Digisonde); over Jicamarca (−2.4º) and São Luís (5.8º), f_oF_2 was difficult to determine in some nighttime hours due to the presence of spread-F; over Cachoeira Paulista (−14.0º) and Santa Maria (−20.5º) the gaps before sunrise are caused by the decrease in F region electron density when the Digisonde could not detect the signals; and the presence of intense Es layers observed (not shown here) in all stations during the storm blocked the signals from the upper ionosphere in some hours.

The ICME shock at 2:00 UT on August 25 did not cause a sudden geomagnetic impulse (Figure 2f). However, fluctuations observed in the IMF B_z may cause the increase of f_oF_2 with respect to the quiet values over Jicamarca (Figure 3a) and São Luís (Figure 4c) during nighttime hours, which made the ionosphere be detected in the ionograms when it usually disappears during geomagnetically quiet days. The enhancement in electron density was higher over Jicamarca (Df_oF_2 ~75% at 2:00 UT, Figure 2a) as compared to São Luís
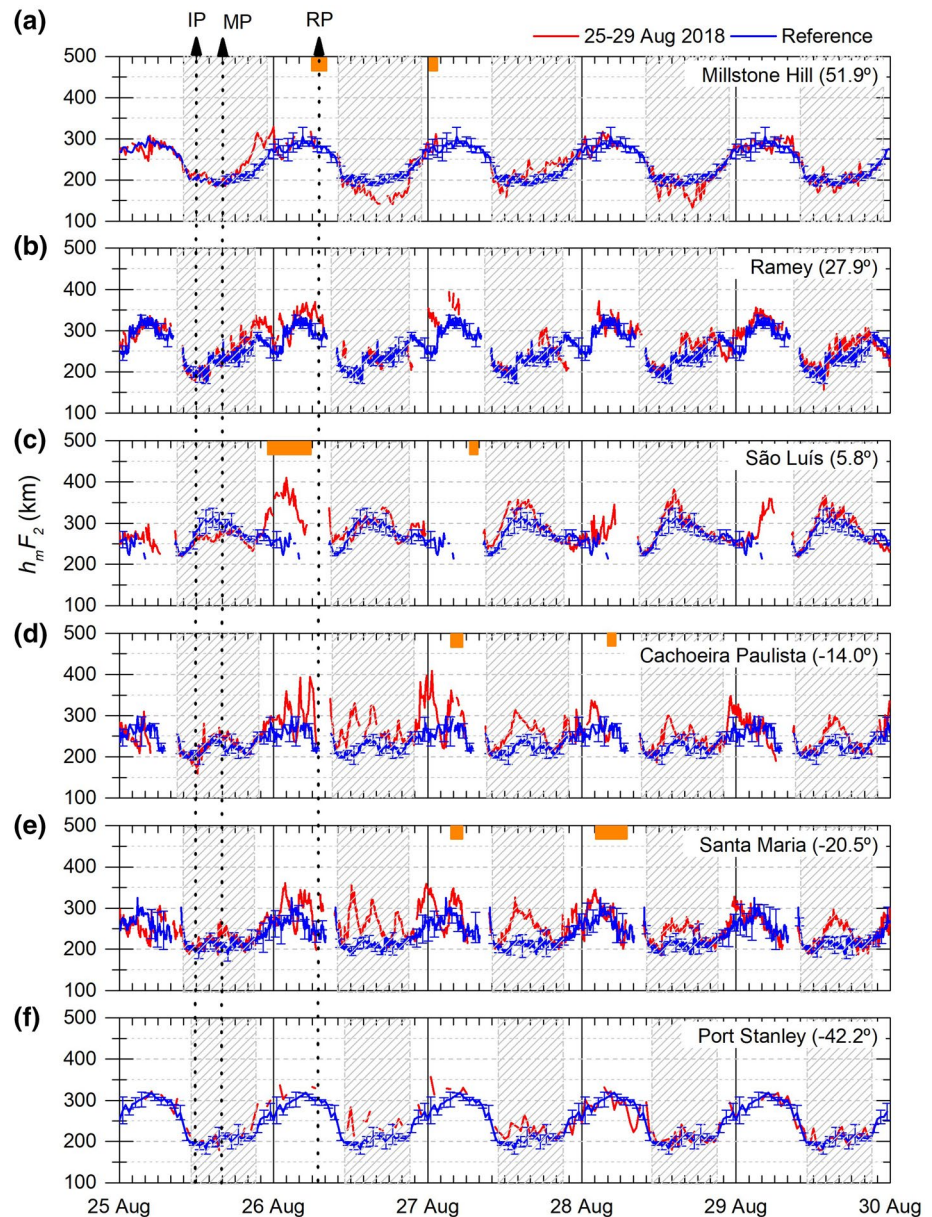
Figure 5. Same as Figure 4 but for h_mF_2. The orange rectangles show the occurrence of spread-F in ionograms.

(Df_oF_2 ~60% at 2:30 UT, Figure 4c), and caused a slight rise in h_mF_2 (Figures 3b and 5c) in both stations. When the ICME material arrived and compressed the magnetosphere at 12:00 UT, there was an increase of ~100 km in h_mF_2 over Jicamarca, which increased ~40% the Dh_mF_2 (Figure 3c) concerning the reference. Interestingly, the response over São Luís was seen as a decrease of Dh_mF_2 of ~20% (Figure 5c).

Further, at the MP (16:00 UT, dayside along 45°W to 76.8°W meridians) when the IMF B_z turned southward, the immediate response of the h_mF_2 over Jicamarca (Figure 3b) is noted as a fast oscillation. The F_2 layer height increased from 330 km (at 16:00 UT) to 360 km (16:15 UT). In the next ionogram collected at Jicamarca, h_mF_2 decreased to 320 km (16:30 UT). The rapid increase at 16:15 UT is a consequence of an undershielding PPEF of eastward polarity. However, h_mF_2 data from São Luís (Figure 5c) did not show enhancements at this time, which would be a characteristic of the PPEF during daytime hours. It means that the PPEF was weak, which may be caused by the unusual gradual beginning of this storm as seen by the smoothed variation of the *SYM-H* index (Figure 2e). This behavior is in line with the difference (*dH*)
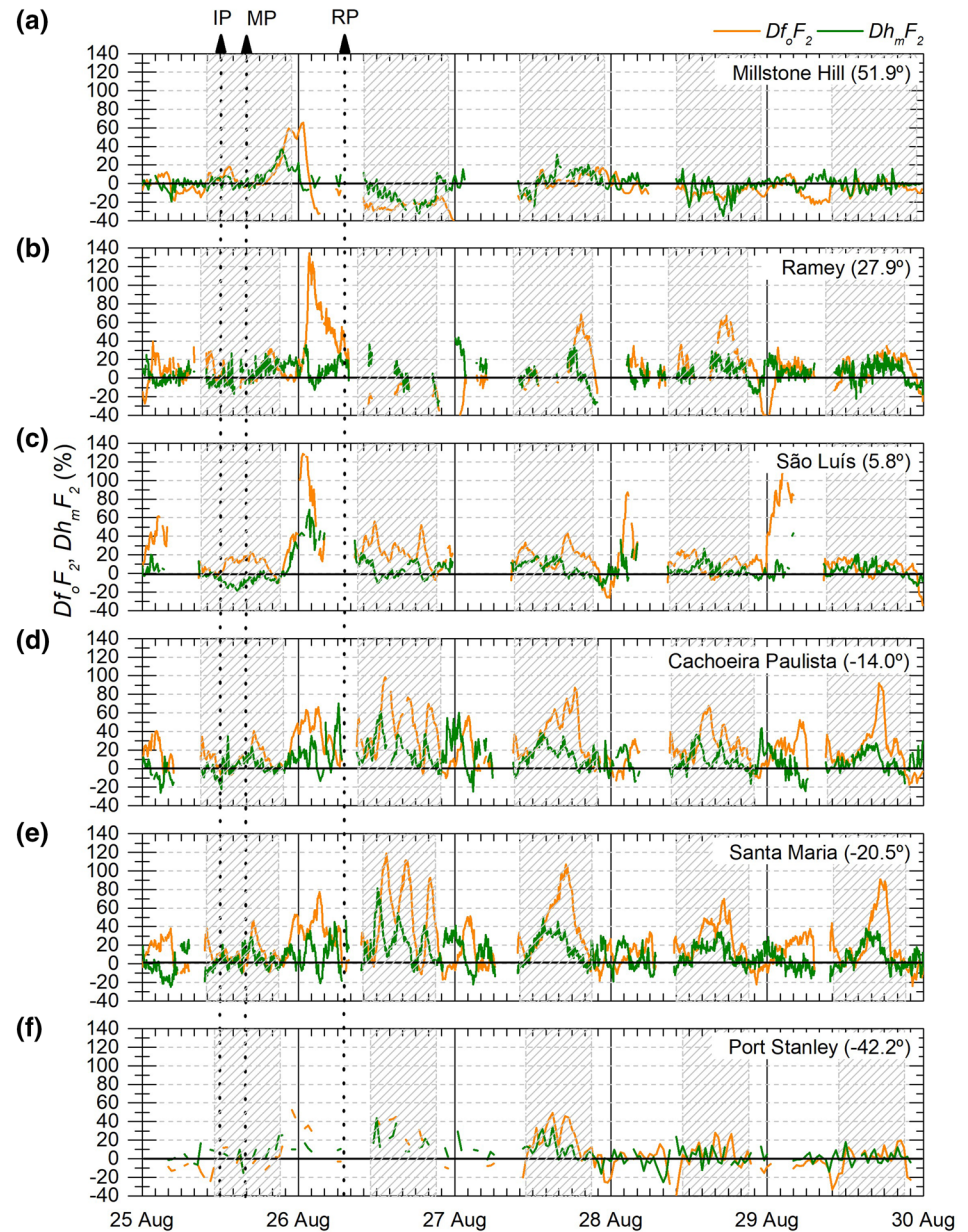
Figure 6. Same as Figure 4 but for the deviations Df_oF_2 (orange line) and Dh_mF_2 (green line).

of the horizontal (*H*-) component computed from two ground-based magnetometers data (Jicamarca and Piura) presented by Astafyeva et al. (2020). The estimated vertical drift velocity of ~40 m/s over São Luís at the beginning of the MP, representing an eastward disturbance electric field of 1 mV/m (not shown here), confirms this fact. However, the action of the undershielding PPEF of eastward polarity seems to be intense enough to enhance the fountain effect and cause the expansion of the southern EIA crest to higher latitudes, as seen by the increase in f_oF_2 over Santa Maria (Figure 4e) 1 h later, at 17:00 UT. The f_oF_2 achieved 7 MHz (an increase of 2 MHz concerning $f_oF_2(q)$). The deviation over Cachoeira Paulista was lower (Df_oF_2 ~35%, Figure 6d) compared to Santa Maria (Df_oF_2 ~50%, Figure 6e).

After ~21:00 UT on August 25, f_oF_2 became higher than $f_oF_2(q)$ at Millstone Hill (Figure 4a). It achieved 8 MHz at 0:45 UT on August 26, when Df_oF_2 rose to 65% (Figure 6a), decreasing to the quiet time levels at 2:00 UT. The positive effect starting at around 21:00 UT seems to be the signature of TIDs reported by

Astafyeva et al. (2020) from the vertical total electron content (VTEC) data estimated by the Global Positioning System (GPS) receiver onboard the Swarm satellite. The authors reported the occurrence of ∼5 TEC unit (TECU; 1 TECU = 10^{16} electrons/m^2) positive storm around 60°N at ∼20:30 UT. Also, they observed similar effects during the next overflies of the satellites around 60ºS at midnight. Nevertheless, such effects were not observed over Port Stanley (Figure 4f).

The TIDs/TADs are one of the physical mechanisms that cause a positive ionospheric storm, as discussed by Prölls (1995) and Danilov (2013). Therefore, the TIDs generated during the storm may have propagated to equatorial latitudes promoting the positive effects in the other stations after ∼22:00 UT on August 25. However, the long-last positive effects over Ramey, São Luís, Cachoeira Paulista, and Santa Maria until ∼6:00 UT on August 26 is not expected to be caused by TIDs during nighttime, i.e., the TIDs may not be the main driver causing these positive effects over these stations. Astafyeva et al. (2020) showed signatures of negative effects at 5:00 UT. As can be seen in Figure 4 from Digisonde data, only positive effects were observed over Ramey, São Luís, Cachoeira Paulista, and Santa Maria. The results from the Port Stanley Digisonde between 1:00 UT and 2:00 UT also indicate the positive effects. The difference between the Digisonde and satellite results from Astafyeva et al. (2020) can be explained considering the variations of h_mF_2 over each station. Note that the positive effects observed with Digisonde data were below 460 km altitude, i.e., below the Swarm altitude.

A tentative explanation of the physical mechanism that caused the positive ionospheric storm in nighttime hours on August 26 is given in terms of h_mF_2 variations over the equatorial and low-latitude stations. The increase of h_mF_2 to > 400 km (Dh_mF_2 ∼50%) over Jicamarca (Figure 3b) after midnight indicates that a disturbing eastward electric field is the main driver acting. This rapid increase is a response to an overshielding condition, which caused the uplift of the F_2 layer and the development of intense spread-F that appeared in the ionogram starting at 0:45 UT on August 26 over Jicamarca, as shown by the orange rectangle in Figure 3b. Over São Luís, the overshielding also caused an increase in h_mF_2 by about 150 km above the quiet time level (2:00 UT on August 26, Figure 5c). It resulted in Dh_mF_2 = 60% (Figure 6c). The layer remained high (>300 km) until 4:40 UT. There is also the presence of spread-F over São Luís, as indicated by the orange rectangle in Figure 5c. It should be noted that the overshielding during nighttime hours on August 26 occurred during the period of IMF $B_z < 0$, unlike the expected northward turning of the IMF B_z. This is probably one of the few observations showing the overshielding process with IMF $B_z < 0$. A similar occurrence of overshielding when the IMF B_z remained southward was reported by Kikuchi et al. (2008) during the November 6, 2001 geomagnetic storm.

It is also noticeable the large height increases/fluctuations over Santa Maria (Figure 5e) and Cachoeira Paulista (Figure 5d) at 2:00 UT, 4:00 UT, and 6:00 UT compared to São Luís (Figure 5c). This response in h_mF_2 seems to be caused by strong equatorward wind. Similar behavior was reported by Abdu et al. (2007) on 28 October 2013 geomagnetic storm, when the h_mF_2 fluctuations/oscillations over Cachoeira Paulista were not observed over São Luís. In the same work, Abdu et al. (2007) observed the development of the EIA due to both conditions of PPEF in the Brazilian sector, similar to what is observed over Cachoeira Paulista and Santa Maria in this work as an enhancement in electron density during these nighttime hours.

The F region responses in the American sector became highly asymmetric between the NH and SH during the RP, which started at 7:00 UT on August 26. As seen from Figure 4a, f_oF_2 presented a salient negative phase at Millstone Hill after sunrise. During daytime hours, f_oF_2 remained below 4 MHz between 10:00 UT and 23:30 UT. The layer substantially decreased to 140 km at 16:30 UT on August 26 (Figure 5a). The lowest value of Dh_mF_2 equal to −30% occurred at 18:30 UT (Figure 6a). The f_oF_2 did recover to the undisturbed mean values after 10:00 UT on August 27. The negative effect was also observed over Ramey, and persisted for more than 20 h, from 10:30 UT on August 26 to 6:00 UT on August 27. During this period, f_oF_2 stayed below 5 MHz most of the time, as shown in Figure 4b, despite the significant gaps caused by the strong Es layers occurrences.

According to the current understanding, the negative ionospheric storm arises from changes in the thermospheric composition generated during storm time at auroral latitudes that increase the N_2 with a reduction in O. The ionospheric and thermospheric effects on August 26 using GUVI/TIMED data were presented by Astafyeva et al. (2020). They show that the satellite flew over the American sector on August 26 between
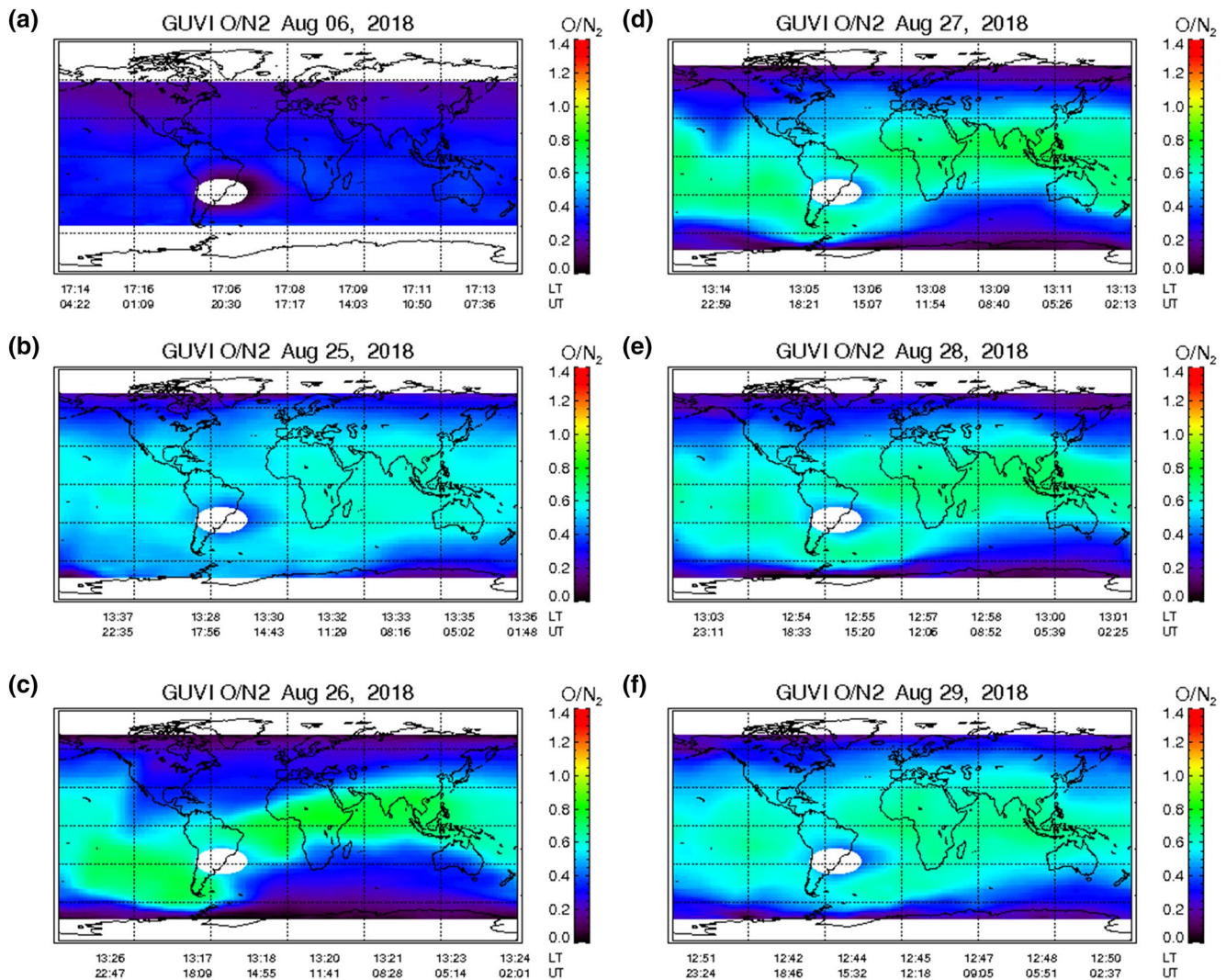
Figure 7. Global maps of the thermospheric [O]/[N₂] ratio derived from TIMED/GUVI (a) on the quiet day of August 6, 2018 and (b–f) during the August 25–29, 2018 geomagnetic storm. GUVI, Global ultraviolet imager; TIMED, Thermosphere Ionosphere Mesosphere Energetics and Dynamics.

~16:30 UT and ~21:30 UT. In their Figure 5 (row A) it is clear the depletion in the thermospheric $[O]/[N_2]$ ratio in the NH. Such depletions are observed below ~50ºS in the SH as well. The thermospheric $[O]/[N_2]$ ratio largely exceeded the reference level at latitudes between ~5ºN and ~60ºS.

The maps of the thermospheric $[O]/[N_2]$ ratio obtained by GUVI/TIMED satellite between August 25 and 29, 2018 are presented in Figure 7. The August 6 (Figure 7a) is taken as reference (control) day. The maps are the result of an interpolated product. The white oval in South America marks the SAMA location, where energetic particles contaminate the detectors and, consequently, significant increases in the noise occur, i.e., the data are not useful in this area. On August 25 (Figure 7b), the $[O]/[N_2]$ ratio was enhanced compared to the reference day (Figure 7a). It is seen from Figure 7c that the thermospheric $[O]/[N_2]$ ratio was significantly increased on August 26 as compared to the previous day. A big enhanced $[O]/[N_2]$ ratio spot converged around the equator from Asia to African sectors and it covered the whole of South America. On the other hand, the ionosphere over Millstone Hill and Ramey were characterized by a decrease in $[O]/[N_2]$ ratio as compared to the previous day. This behavior explains the observed negative effects over Millstone Hill and Ramey on August 26 in Figures 4a and 4b. This fact also occurred in the European sector, where negative ionospheric effects were observed at all latitudes during the RP, as reported by Blagoveshchensky and Sergeeva (2020). According to these authors, the negative effects were caused by the decrease of $[O]/[N_2]$.

Regarding the stations located in the SH on August 26, it is observed only positive ionospheric storm. The increase of the f_oF_2 concerning the quiet days is explained in part by the enhanced thermospheric $[O]/[N_2]$ ratio (Figure 7c). However, the main feature observed over São Luís, Cachoeira Paulista, and Santa Maria during daytime is four peaks in f_oF_2 that may be caused by a rapid mechanism such as an electrodynamic one. As shown in Figure 2d, these peaks appear in phase with successive intensifications in the IMF B_z and IEF E_y (marked with 1, 2, 3, and 4 in Figure 2d). These peaks might occur in f_oF_2 over Port Stanley, but with substantially lower amplitudes (the peaks are difficult to detect due to the lack of measurements). Note also the several oscillations in the *ASY-H* index in Figure 2f. Huang et al. (2005) reported that fluctuations in the *AE* index under IMF B_z south conditions cause PPEF (see also Abdu et al., 2007). Interestingly, h_mF_2 values over Cachoeira Paulista and Santa Maria also exhibited similar peaks as observed in f_oF_2 but ~1 h before. Considering a competition between these two drivers (thermospheric composition shown in Figure 7 and disturbed electric fields), the decrease of $[O]/[N_2]$ in the NH causing the negative effects was more effective than the disturbing electric fields (no peaks in f_oF_2 are observed). To sum up, the positive storm effects observed over the stations in the SH on August 26 seem to be occurred by the combined effect of the enhanced thermosphere $[O]/[N_2]$ ratio and the PPEF process (which dominated over the expected DDEF effects). It is also remarkable that in terms of Df_oF_2, the highest peaks occurred over Santa Maria, achieving 120% at 13:30 UT, 112% at 16:30 UT, and 95% at 20:15 UT.

On the following days of the RP, it would be expected a control of the thermospheric compositions and DDEF in the *F* region responses causing negative storm effects, as observed in the case presented by Abdu et al. (2007) or Balan et al. (2013). However, f_oF_2 was higher than the quiet time pattern over all stations except Millstone Hill (which recovery faster), i.e., in general, the plasma density was larger in the EIA regions, and it was roughly hemispherically symmetric. Interestingly, Santa Maria and Cachoeira Paulista presented remarkably f_oF_2 enhancements at 14:00–20:00 UT on August 27–29, whereas the f_oF_2 over São Luís did not show significant changes. The Df_oF_2 achieved 107% at 17:05 UT over Santa Maria (Figure 6e) and 87% at 18:30 UT over Cachoeira Paulista (Figure 6d) on August 27. On the same day, Df_oF_2 achieved 70% at 19:25 UT over Ramey (Figure 6b) and 50% at 15:00 UT over Port Stanley (Figure 6f). In the next two days, August 28 and 29, positive effects are still clearly noticed over Santa Maria, Cachoeira Paulista, and less evident over Ramey and Port Stanley. Moreover, note that the enhanced thermospheric $[O]/[N_2]$ ratio is still sustained over South America during the RP, as shown in the maps of Figures 7d–7f. As the storm progressed, the neutral composition changes extended to higher latitudes.

To illustrate the enhancement of the plasma density in South America during the geomagnetic storm, it is shown a set of TEC maps from 14:30 UT to 17:00 UT in Figure 8. The curved solid line in each map represents the geomagnetic equator. The methodology applied to generate these TEC maps can be found in detail in Takahashi et al. (2016). These maps have a spatial resolution in latitude and longitude of $0.5º \times 0.5°$. The TEC maps during the reference quiet day (August 6, 2018-08-06) are shown in the first row of Figure 8. During the reference day, the EIA developed at 14:30 UT, as seen on the eastern coast (around 30º–40ºW) of Brazil. In the following maps of the first row, the plasma density is enhanced in the equatorial and low latitude regions in Brazil (0º–15ºS), which correspond to the southern EIA crest. The most intense patches of TEC are identified around 15ºS at 16:00 UT. Then, the TEC decreased until around 22:30 UT (not shown here). Indeed, this reference quiet day represents well the average daily behavior of the EIA during winter in the SH, as discussed in Takahashi et al. (2016).

The EIA became stronger during the RP (2018-08-27, 2018-08-28, 2018-08-29), as observed by the second, third, and fourth row of Figure 8, respectively, as compared to the reference quiet day (first row). The largest enhancement of plasma density is observed all over the Brazilian territory in the maps correspondent to 27 August. Regions with TEC > 30 are very clear between 30º and 60ºW in the maps after 15:30 UT achieving a wider area. It is observed TEC ≥ 25 over Santa Maria (~30ºS) and Cachoeira Paulista (14º S) after 15:30 UT on August 27, which means a strong development of the southern EIA crest farther from the magnetic equator as compared to the reference quiet day. Small enhancement in plasma density is also observed over Port Stanley (~42ºS). The TEC slightly decreased on the following days, August 28–29, but it is still intense compared with the geomagnetically quiet day (August 6). It is still possible to observe large enhancements of plasma density (TEC > 30) from 15:00 UT to 16:30 UT on August 28, and from 15:30 UT to 16:00 UT on
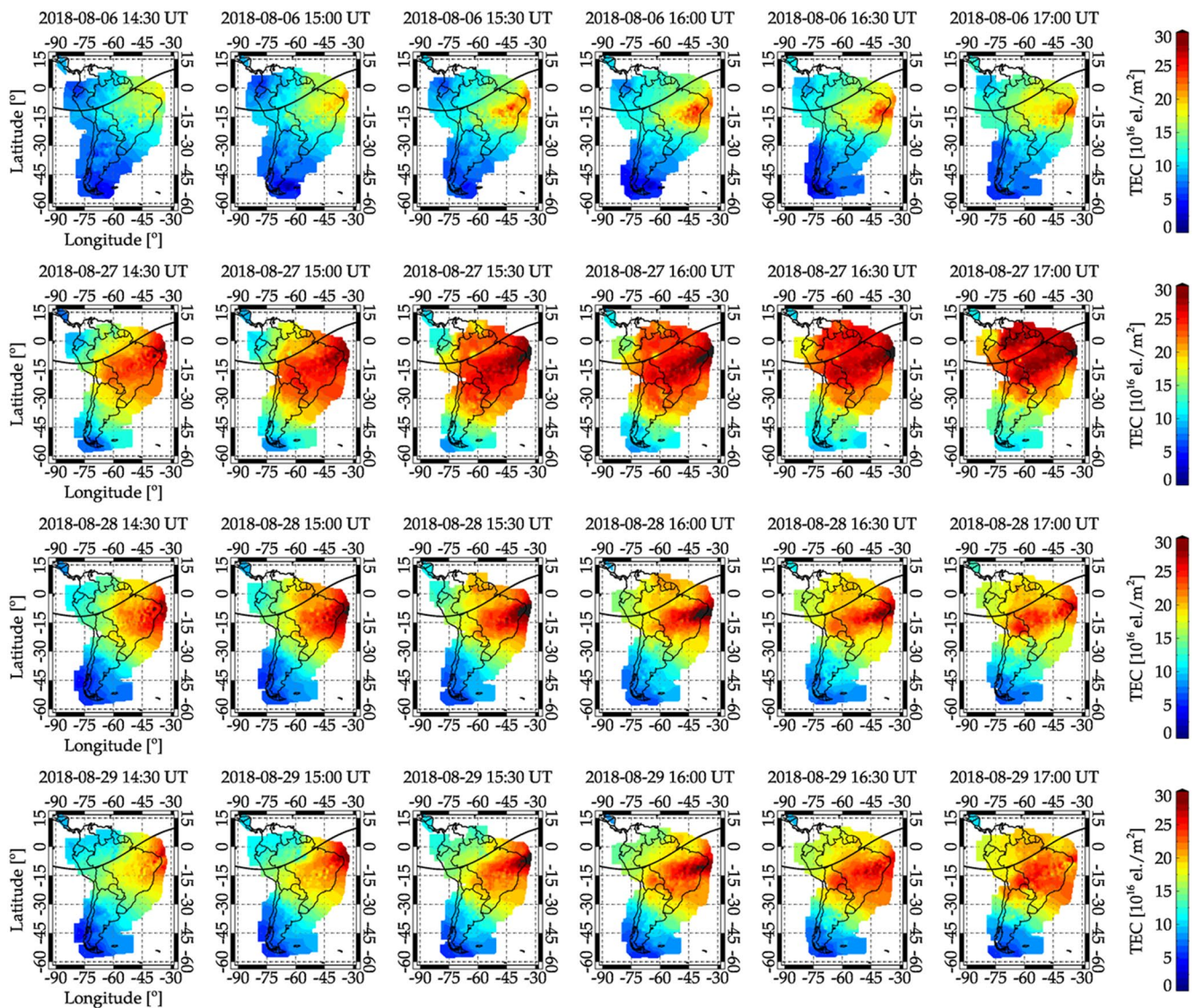
Figure 8. Sequence of TEC maps over South America from 14:30 UT to 17:00 UT on the quiet day of August 6, 2018 (first row) and during the August 27, 28, and 29, 2018 (second, third, and fourth row, respectively). The color scale indicates the TEC intensity. The curved solid line in each map is the geomagnetic equator. TEC, total electron content.

August 29. Overall, the maps show no suppression/weakening of dayside EIA, which indicates no DDEF effects on TEC (and Digisonde) data during the RP (August 27–29, 2018) of the geomagnetic storm.

Lissa et al. (2020) studied the ionosphere responses on August 25, 2018 geomagnetic storm using TEC data from GPS stations distributes over India, Sri Lanka, China, Taiwan, and the Philippines. The authors also observed large positive effects in the daytime hours for three consecutive days from August 26 to 29. They explained the drivers of the positive effects in terms of the recombination process, plasma diffusion caused by disturbed winds and enhanced thermospheric $[O]/[N_2]$ ratio over the considered longitudes (80ºE–120ºE). In addition to these drivers, it is also suggested in the present work that the HSS had the potential to play a key role in causing the positive effects during the RP. The daytime intensification of the EIA may be caused by PPEF of eastward polarity, which in turn, depends on the IMF B_z component. Wei et al. (2008) explained that the PPEF can be classified into "single penetration" and "multiple penetrations". The former is characterized by a southward or northward abrupt reversal of the IMF B_z component, and the latter is the oscillation between northward and southward directions. The alternating polarity in the IMF B_z component

shown in Figure 2d could excite discontinuous magnetic reconnection. As shown before, IEF E_y component is controlled by solar wind speed as $E_y = (V_x)(B_z)$, which peaked 630 km/s at 17:00 UT on August 27 (Figure 2c). Therefore, it is suggested that the high V_{SW} effectively contributed to the enhancement of the PPEF (eastward polarity). As a result, it was observed positive ionospheric effects centered at around ±15°–±30° magnetic latitudes (note that there is no station at +15º magnetic latitude) due to the PPEF. It explains the higher Df_oF_2 peaks observed over Santa Maria as compared to Cachoeira Paulista during the RP.

In a recent work, Ren et al. (2020) used TEC data collected by the Beidou geostationary satellites to study the impact of the HSS in the ionosphere during August 27–29, 2018. Using multiple observations and the Thermosphere-ionosphere-electrodynamics general circulation model (TIEGCM), the authors suggested that the HSS modulates the low latitude ionosphere during the RP. The TIEGCM could well reproduce the positive ionospheric storm during the RP, although it underestimated the TEC enhancements.

Denton et al. (2009) reported that during the passage of a typical HSS over the magnetosphere, it induces several phenomena. Therefore, it is important to understand the impact of this HSS to identify the main dynamic mechanisms responsible for the long-last intense positive ionospheric effects in Digisonde data over Santa Maria and Cachoeira Paulista on August 27–29. Thereby, a close inspection from August 27 in the IMF features through the linear correlation calculated between the variation of the solar wind velocity components at L1 location (ACE data) versus the corresponding Alfvén velocity components (figures not shown) confirms that the fluctuations are Alfvénic. Alfvénic fluctuations may also occur concomitantly with the southward IMF B_z (Gonzalez et al., 1994) and can start the reconnection in the Earth's magnetosphere, which can trigger the main drives to moderate geomagnetic storms (Tsurutani et al., 1995), followed by a sequence of the substorms, as observed on August 27–29. Substorms are an important process for the injection of low energy electron particles in the inner magnetosphere (Jaynes et al., 2015). Substorms accompanied by the IMF B_z and IMF Alfvénic fluctuations play a crucial role in generating Ultralow Frequency (ULF) waves in the magnetosphere, consequently, may occur wave-particle interaction (Da Silva et al., 2019). This dynamic in the magnetosphere observed during the influences of these Alfvénic fluctuations associated with HSS in the study agrees with the results discussed by Denton et al. (2009). As far as the author's know, it seems to be the first time that these results are discussed in this geomagnetic storm.

Denton et al. (2009) also reported that disturbed f_oF_2 and h_mF_2 values last for at least 4 days in the middle latitudes. Therefore, the HSS on August 26 seems to be one of the factors that caused the long-last intense positive ionospheric storm effects in Digisonde data over Santa Maria and Cachoeira Paulista between August 27 and 29, and over Ramey (summer) in a less degree of intensity. Santa Maria and Cachoeira Paulista stations are in the winter, which is well known that positive phases show a maximum occurrence. However, the effects reported here were quite dramatic due to the complex drivers acting during the geomagnetic storm.

The results presented in this work show that the F_2 layer electron density was significantly disturbed during the MP and (especially) in the RP. Moreover, the southern EIA crest achieved the Santa Maria region as seen in f_oF_2 and confirmed in TEC data. It caused the most pronounced positive effects in the electron density with respect to all stations analyzed here. Despite being an intense geomagnetic storm, the EIA was not suppressed due to the DDEF process during the RP. Finally, this work shows how unpredictable is the storm-time ionosphere, especially in the SAMA region, which is an additional difficulty imposed in the analysis of the I-T system responses and the development of models.

5. Conclusions

The data from the new Digisonde station in Santa Maria were used for the first time in this work to study a geomagnetic storm. The August 25–29, 2018 storm is the third most intense of the Solar Cycle 24 and is considered complex due to the interaction of the two consecutive ICMEs and followed by a HSS. The responses of the F_2 layer are studied considering the critical frequency f_oF_2 and its peak height h_mF_2. The plasma parameters are compared with data from the Digisondes installed at Millstone Hill, Ramey, Jicamarca, São Luís, Cachoeira Paulista, and Port Stanley in the NH and SH in the American sector. The observed positive

and negative ionospheric storm effects are quantified by the deviation of f_oF_2 (Df_oF_2) and h_mF_2 (Dh_mF_2) in percent.

The results show that the development of negative and positive phases had different durations, intensities, and onset. In general, the F region behavior displayed a remarkable asymmetry in the response of the geomagnetic disturbances during the RP. The main conclusions of the study are as follows:

1. At the beginning of the MP (16:00 UT on August 25), the increases in the F_2 layer height over Jicamarca and São Luís are a response to a weak undershielding PPEF of eastward polarity. Further, on August 25–26 during the MP, the positive ionospheric effects were observed in all stations and could be caused by several factors. During the daytime hours on August 25, the increase in electron density over Millstone Hill seems to be an effect of TIDs at higher latitudes, which may propagate equatorward. The effect of an overshielding process could be noticed after sunset as an increase of the h_mF_2 in Jicamarca and São Luís. Consequently, the effects of positive ionospheric storms were observed in middle and low latitudes due to the development of the EIA crests. Interestingly, the overshielding during nighttime hours on August 26 occurred when IMF $B_z < 0$. However, it is expected to occur during the northward turning of the IMF B_z. This work is probably one of the few cases showing the overshielding process with IMF $B_z < 0$

2. Significant modifications in the neutral composition and electron density were noticed on August 26 during the prolonged southward IMF B_z component. Large electron density reduction was observed over Millstone Hill and Ramey as a consequence of a decrease in the thermospheric $[O]/[N_2]$. One the other hand, it was observed enhancement in the electron density in the SH stations caused mainly by an increase in $[O]/[N_2]$. Besides, several oscillations in f_oF_2 were observed in the SH almost in phase with IMF B_z (and IEF E_y) component increasing, even more, the positive phase, which resulted in higher deviations in Df_oF_2 and Dh_mF_2. However, such oscillations were not observed over Millstone Hill and Ramey due to the strong decrease in electron density and its peak height. The interaction of the two mechanisms (changes in the thermospheric composition and electric field) had the potential to play a key role in supporting the large F_2 layer electron density on August 26 over the stations in the SH

3. The incidence of the HSS seems to modulate the Earth's magnetosphere and could disturb the middle latitude ionosphere in the SH (especially) for multiple days, from August 27 to 29 during the RP. A close analysis of the IMF features on August 27 through the linear correlation between the variation of the solar wind velocity components and the corresponding Alfvén velocity components confirm that the fluctuations are Alfvénic in nature. This is one important result since it helps to explain the intensification of the EIA crests over Santa Maria in terms of f_oF_2 and TEC data during daytime hours from August 27 to 29

4. During the RP, the highest deviations were always observed over Santa Maria due to the changes in the southern EIA crest position

Finally, the results show how unpredictable is the storm-time ionosphere over Santa Maria and, in general, in the wide region close to the SAMA center, which presents an additional complication in understanding the I-T responses and the development of models in a region with an anomalously weak geomagnetic field.

Data Availability Statement

The GUVI data used here (http://guvitimed.jhuapl.edu/) are provided through support from the NASA MO&DA program. The Santa Maria Digisonde data can be also downloaded upon registration at the Embrace webpage from INPE Space Weather Program (http://www2.inpe.br/climaespacial/portal/en). The Digisonde data are provided by GIRODidbase (http://umlcar.uml.edu/).

References

Abdu, M. A., Batista, I. S., Carrasco, A. J., & Brum, C. G. M. (2005). South Atlantic magnetic anomaly ionization: A review and a new focus on electrodynamics effects in the equatorial ionosphere. *Journal of Atmospheric and Solar-Terrestrial Physics*, *67*, 1643–1657. https://doi.org/10.1016/j.jastp.2005.01.014

Abdu, M. A., de Paula, E. R., Batista, I. S., Reinisch, B. W., Matsuoka, M. T., CamargoVeliz, P. O. O., et al.(2008). Abnormal evening vertical plasma drift and effects on ESF and EIA over Brazil-South Atlantic sector during the 30 October 2003 super storm. *Journal of Geophysical Research*, *113*, A07313. https://doi.org/10.1029/2007JA012844

Abdu, M. A., Kherani, E. A., Batista, I. S., & Sobral, J. H. A. (2009). Equatorial evening prereversal vertical drift and spread F suppression by disturbance penetration electric fields. *Geophysical Research Letters*, *36*, L19103. https://doi.org/10.1029/2009GL039919

Abdu, M. A., Maruyama, T., Batista, I. S., Saito, S., & Nakamura, M. (2007). Ionospheric responses to the October 2003 superstorm: Longitude/local time effects over equatorial low and middle latitudes. *Journal of Geophysical Research: Space Physics*, *112*, A10306. https://doi.org/10.1029/2006JA012228

Abunin, A. A., Abunina, M. A., Belov, A. V., & Chertok, I. M. (2020). Peculiar solar sources and geospacer disturbances on 20-26 August 2018. *Solar Physics*, *295*, 7. https://doi.org/10.1007/s11207-019-1574-8

Alves, L. R., Da Silva, L. A., Souza, V. M., Sibeck, D. G., Jauer, P. R., Vieira, L. E. A., et al. (2016). Outer radiation belt dropout dynamics following the arrival of two interplanetary coronal mass ejections. *Geophysical Research Letters*, *43*, 978–987. https://doi.org/10.1002/2015GL067066

Astafyeva, E., Bagiya, M. S., Förster, M., & Nishitani, N. (2020). Unprecedented hemispheric asymmetries during a surprise ionospheric storm: A game of drivers. *Journal of Geophysical Research: Space Physics*, *125*, e2019JA027261. https://doi.org/10.1029/2019JA027261

Balan, N., & Bailey, G. J. (1995). Equatorial plasma fountain and its effects: Possibility of an additional layer. *Journal of Geophysical Research*, *100*(A11), 21421–21432.

Balan, N., Otsuka, Y., Nishioka, M., Liu, J. Y., & Bailey, G. J. (2013). Physical mechanisms of the ionospheric storms at equatorial and higher latitudes during the recovery phase of geomagnetic storms. *Journal of Geophysical Research: Space Physics*, *118*, 2660–2669. https://doi.org/10.1002/jgra.50275

Balan, N., Souza, J., & Bailey, G. J. (2017). Recent developments in the understanding of equatorial ionization anomaly: A review. *Journal of Atmospheric and Solar-Terrestrial Physics*, *171*, 3–11. https://doi.org/10.1016/j.jastp.2017.06.020

Blagoveshchensky, D. V., & Sergeeva, M. A. (2020). Ionospheric parameters in the European sector during the magnetic storm of August 25-26, 2018. *Advances in Space Research*, *65*, 11–18. https://doi.org/10.1016/j.asr.2019.07.044

Blanc, M., & Richmond, A. D. (1980). The ionospheric disturbance dynamo. *Journal of Geophysical Research*, *85*, 1669–1686. https://doi.org/10.1029/JA085iA04p01669

Christensen, A. B., Paxton, L. J., Avery, S., Craven, J., Crowley, G., Humm, D. C., et al. (2003). Initial observations with the Global Ultraviolet Imager (GUVI) on the NASA TIMED satellite mission. *Journal of Geophysical Research*, *108*(A12), 1451. https://doi.org/10.1029/2003JA009918

Chulliat, A., Brown, W., Alken, P., Beggan, C., Nair, M., Cox, G., et al. (2020). *The US/UK World magnetic model for 2020-2025: Technical report*, Boulder, CO: National Centers for Environmental Information, NOAA. https://doi.org/10.25923/ytk1-yx35

Da Silva, L. A., Sibeck, D., Alves, L. R., Souza, V. M., Jauer, P. R., Claudepierre, S. G., et al. (2019). Contribution of ULF wave activity to the global recovery of the outer radiation belt during the passage of a high-speed solar wind stream observed in September 2014. *Journal of Geophysical Research: Space Physics*, *124*, 1660–1678. https://doi.org/10.1029/2018JA026184

Danilov, A. D. (2013). Ionospheric F-region response to geomagnetic disturbances. *Advances in Space Research*, *53*(3), 343–366. https://doi.org/10.1016/j.asr.2013.04.019

Denardini, C. M., Dasso, S., & Gonzalez-Esparza, J. A. (2016). Review on space weather in Latin America. 2. The research networks ready for space weather. *Advances in Space Research*, *58*(10), 1940–1959. https://doi.org/10.1016/j.asr.2016.03.013

Denton, M. H., Ulich, T., & Turunen, E. (2009). Modification of midlatitude ionospheric parameters in the F_2 layer by persistent high-speed solar wind streams. *Space Weather*, *7*, S04006. https://doi.org/10.1029/2008SW000443

Fagundes, P. R., Cardoso, F. A., Fejer, B. G., Venkatesh, K., Ribeiro, B. A. G., & Pillat, V. G. (2016). Positive and negative GPS-TEC ionospheric storm effects during the extreme space weather event of March 2015 over the Brazilian sector. *Journal of Geophysical Research: Space Physics*, *121*, 5613–5625. https://doi.org/10.1002/2015JA022214

Fuller-Rowell, T. J., Codrescu, M. V., Rishbeth, H., Moffett, R. J., & Quegan, S. (1996). On the seasonal response of the thermosphere and ionosphere to geomagnetic storms. *Journal of Geophysical Research: Space Physics*, *101*, 2343–2353. https://doi.org/10.1029/95JA01614

Gonzalez, W. D., Joselyn, J. A., Kamide, Y., Kroehl, H. W., Rostoker, G., Tsurutani, B. T., & Vasyliunas, V. M. (1994). What is a magnetic storm? *Journal of Geophysical Research*, *99*(A4), 5771–5792.

Habarulema, J. B., Katamzi-Joseph, Z. T., Burešová, D., Nndanganeni, R., Matamba, T., Tshisaphungo, M., et al. (2020). Ionospheric response at conjugate locations during the 7–8 September 2017 geomagnetic storm over the Europe-African longitude sector. *Journal of Geophysical Research: Space Physics*, *125* e2020JA028307. https://doi.org/10.1029/2020JA028307

Huang, C. S., Foster, J. C., Goncharenko, L. P., Erickson, P. J., Rideout, W., & Coster, A. J. (2005). A strong positive phase of ionospheric storms observed by the Millstone Hill incoherent scatter radar and global GPS network. *Journal of Geophysical Research*, *110*, A06303. https://doi.org/10.1029/2004JA010865

Jaynes, A. N., Baker, D. N., Singer, H. J., Rodriguez, J. V., Loto'aniu, T. M., Ali, A. F., et al. (2015). Source and seed populations for relativistic electrons: Their roles in radiation belt changes. *Journal of Geophysical Research: Space Physics*, *120*, 7240–7254. https://doi.org/10.1002/2015JA021234

Jones, A. D., Kanekal, S. G., Baker, D. N., Klecker, B., Looper, M. D., Mazur, J. E., & Schiller, Q. (2017). SAMPEX observations of the South Atlantic anomaly secular drift during solar cycles 22–24. *Advances in Space Research*, *15*, 44–52. https://doi.org/10.1002/2016SW001525

Kelley, M. C., Fejer, B. G., & Gonzales, C. A. (1979). An explanation for anomalous equatorial ionospheric electric fields associated with a northward turning of the interplanetary magnetic field. *Geophysical Research Letters*, *6*, 301–304. https://doi.org/10.1029/GL006i004p00301

Kikuchi, T., Hashimoto, K. K., & Nozaki, K. (2008). Penetration of magnetospheric electric fields to the equator during a geomagnetic storm. *Journal of Geophysical Research*, *113*, A06214. https://doi.org/10.1029/2007JA012628

Kikuchi, T., Liihr, H., Schlegel, K., Tachihara, H., Shinohara, M., & Kitamura, T.-I. (2000). Penetration of auroral electric fields to the equator during a substorm. *Journal of Geophysical Research*, *105*(A10), 23251–23261.

Kurnosova, L. V., Kolobyanina, T. N., Logachev, V. I., Razorenov, L. A., Sirotkin, I. A., & Fradkin, M. I. (1962). Discovery of radiation anomalies above the South Atlantic at heights of 310–340 km. *Planetary and Space Science*, *9*(8), 513–516. https://doi.org/10.1016/0032-0633(62)90057-0

Lee, C. C., Reinisch, B. W., Su, S.-Y., & Chen, W. S. (2008). Quiet-time variations of F2-layer parameters at Jicamarca and comparison with IRI-2001 during solar minimum. *Journal of Atmospheric and Solar-Terrestrial Physics*, *70*(1), 184–192. https://doi.org/10.1016/j.jastp.2007.10.008

Li, G., Ning, B., Hu, L., Liu, L., Yue, X., Wan, W., et al. (2010). Longitudinal development of low-latitude ionospheric irregularities during the geomagnetic storms of July 2004. *Journal of Geophysical Research*, *115*, A04304. https://doi.org/10.1029/2009JA014830

Lissa, D., Srinivasu, V. K. D., Prasad, D. S. V.V. D., & Niranjan, K. (2020). Ionospheric response to the 26 August 2018 geomagnetic storm using GPS-TEC observations along 80°E and 120°E longitudes in the Asian sector. *Advances in Space Research*, *66*(6), 1427–1440. https://doi.org/10.1016/j.asr.2020.05.025

Matamba, T. M., Habarulema, J. B., & McKinnell, L.-A. (2015). Statistical analysis of the ionospheric response during geomagnetic storm conditions over South Africa using ionosonde and GPS data. *Space Weather*, *13*, 536–547. https://doi.org/10.1002/2015SW001218

Moro, J., Denardini, C. M., Abdu, M. A., Correia, E., Schuch, N. J., & Makita, K. (2012). Latitudinal dependence of cosmic noise absorption in the ionosphere over the SAMA region during the September 2008 magnetic storm. *Journal of Geophysical Research*, *117*, A06311 https://doi.org/10.1029/2011JA017405

Moro, J., Denardini, C. M., Abdu, M. A., Correia, E., Schuch, N. J., & Makita, K. (2013). Correlation between the cosmic noise absorption calculated from the SARINET data and energetic particles measured by MEPED: Simultaneous observations over SAMA region. *Advances in Space Research*, *51*, 11692–11700.

Moro, J., Resende, L. C. A., Denardini, C. M., Xu, J., Batista, I. S., Andrioli, V. F., & Schuch, N. J. (2017). Equatorial E region electric fields and sporadic E layer responses to the recovery phase of the November 2004 geomagnetic storm. *Journal of Geophysical Research: Space Physics*, *122*, 12517–12533. https://doi.org/10.1002/2017JA024734

Moro, J., Xu, J., Denardini, C. M., Resende, L. C. A, Silva, R. P., Chen, S. S., et al. (2020). Performance of the IRI-2016 over Santa Maria, a Brazilian low-latitude station located in the central region of the South American Magnetic Anomaly (SAMA). *Annales Geophysicae*, *38*, 457–466. https://doi.org/10.5194/angeo-38-457-2020

Moro, J., Xu, J., Denardini, C. M., Resende, L. C. A, Silva, R. P., Liu, Z., et al. (2019). On the sources of the ionospheric variability in the South American Magnetic Anomaly during solar minimum. *Journal of Geophysical Research: Space Physics*, *124*, 7638–7653. https://doi.org/10.1029/2019JA026780

Paxton, L. J., Christensen, A. B., Humm, D. C., Ogorzalek, B. S., Pardoe, C. T., Morrison, D., et al. (2005). Global ultraviolet imager (GUVI): Measuring composition and energy inputs for the NASA Thermosphere Ionosphere Mesosphere Energetics and Dynamics (TIMED) mission. *Proceedings of the SPIE 3756, Optical Spectroscopic Techniques and Instrumentation for Atmospheric and Space Research III*, 20 October 1999. https://doi.org/10.1117/12.366380

Prölss, G. W. (1995). Ionospheric F-region storms. In H. Volland (Ed.), Handbook of atmospheric electrodynamics. (Vol: 2, pp. 195–248). Boca Raton, FL: CRCpress.

Reinisch, B., & Galkin, I. (2011). Global ionospheric radio observatory (GIRO). *Earth, Planets and Space*, *63*, 377–381. https://doi.org/10.5047/eps.2011.03.001

Ren, D., Lei, J., Zhou, S., Li, W., Huang, F., Luan, X., et al. (2020). High-speed solar wind imprints on the ionosphere during the recovery phase of the August 2018 geomagnetic storm. *Space Weather*, *18*, e2020SW002480. https://doi.org/10.1029/2020SW002480

Resende, L. C. A., Batista, I. S., Denardini, C. M., Carrasco, A. J., Andrioli, V. F., Moro, J., et al. (2016). Competition between winds and electric fields in the formation of blanketing sporadic E layers at equatorial regions. *Earth, Planets and Space*, *68*, 201. https://doi.org/10.1186/s40623-016-0577-z

Richardson, I. G., & Cane, H. V. (2010). Near-Earth interplanetary coronal mass ejections during solar cycle 23 (1996–2009): Catalog and summary of properties. *Solar Physics*, *264*(1), 189–237. https://doi.org/10.1007/s11207-010-9568-6

Schuch, N. J., Durão, O. S. C., da Silva, M. R., Mattiello-Francisco, F., Martins, J. B. S., Legg, A., et al. (2019). The NANOSATC-BR, Cubesat Development Program—A joint Cubesat Program developed by UFSM and INPE/MCTIC Space geophysics mission payloads and first results. *Brazilian Journal of Geophysics*, *37*, 95–103. https://doi.org/10.22564/rbgf.v37i1.1992

Shue, J.-H., Song, P., Russell, C. T., Steinberg, J. T., Chao, J. K., Zastenker, G., et al. (1998). Magnetopause location under extremes solar wind conditions. *Journal of Geophysical Research*, *103*, 17691–17000. https://doi.org/10.1029/98JA01103

Sobral, J. H. A., Abdu, M. A., Yamashita, C. S., Gonzalez, W. D., Clua de Gonzalez, A., Batista, I. S., et al. (2001). Responses of the low-latitude ionosphere to very intense geomagnetic storms. *Journal of Atmospheric and Solar-Terrestrial Physics*, *63*, 965–974. https://doi.org/10.1016/S13646826(00)00197-8

Takahashi, H., Wrasse, C. M., Denardini, C. M., Pádua, M. B., de Paula, E. R., Costa, S. M. A., et al. (2016). Ionospheric TEC Weather Map Over South America. *Space Weather*, *14*, 937–949. https://doi.org/10.1002/2016SW001474

Tsurutani, B., Gonzalez, W. D., Gonzalez, A. L., Tang, F., Arballo, J. K., & Okada, M. (1995). Interplanetary origin of geomagnetic activity in the declining phase of the solar cycle. *Journal of Geophysical Research*, *100*(A11), 21717–21733.

Tsurutani, B., Mannucci, A., Iijima, B., Abdu, M. A., Sobral, J. H. A., Gonzalez, W. D., et al. (2004). Global dayside ionospheric uplift and enhancement associated with interplanetary electric fields. *Journal of Geophysical Research*, *109*, A08302. https://doi.org/10.1029/2003JA010342

Wei, Y., Hong, M., Wan, W., Du, A., Lei, J., Zhao, B., et al. (2008). Unusually long lasting multiple penetration of interplanetary electric field to equatorial ionosphere under oscillating IMF B_z. *Geophysical Research Letters*, *35*, L02102. https://doi.org/10.1029/2007GL032305

Wolf, R. A., Spiro, R. W., Sazykin, S., & Toffoletto, F. R. (2007). How the Earth's inner magnetosphere works: An evolving picture. *Journal of Atmospheric and Solar-Terrestrial Physics*, *69*(3), 288–302. https://doi.org/10.1016/j.jastp.2006.07.026

Yu, T., Ren, Z., Yu, Y., Yue, X., Zhou, X., & Wan, W. (2020). Comparison of reference heights of O/N2 and ∑O/N2 based on GUVI dayside limb measurement. *Space Weather*, *18*, e2019SW002391. https://doi.org/10.1029/2019SW002391

Zhang, Y., Paxton, L. J., Kil, H., Meng, C.-I., Mende, S. B., Frey, H. U., & Immel, T. J. (2003). Negative ionospheric storms seen by the IMAGE FUV instrument. *Journal of Geophysical Research*, *108*(A9), 1343. https://doi.org/10.1029/2002JA009797

Zou, H., Li, C., Zong, Q., Parks, G. K., Pu, Z., Chen, H., et al. (2015). Short-term variations of the inner radiation belt in the South Atlantic anomaly. *Journal of Geophysical Research: Space Physics*, *120*, 4475–4486. https://doi.org/10.1002/2015JA021312